Received: 17 March 2021 | Revised: 19 April 2021 | Accepted: 27 April 2021

DOI: 10.1002/nano.202100131

RESEARCH ARTICLE

Nano Select Open Access WILEY

Luminescence and sensitivity enhancement of oxygen sensors through tuning the spectral overlap between luminescent dyes and SiO_2@Ag nanoparticles

Wenwen Yin[1] | **Jinxing Chen**[2] | **Jiajie Sui**[3] | **Dana Dabiri**[1] | **Guozhong Cao**[3]

[1] Department of Aeronautics & Astronautics, University of Washington, Seattle, Washington, USA

[2] Institute of Functional Nano&Soft Materials (FUNSOM), Jiangsu Key Laboratory for Carbon-Based Functional Materials Devices, Soochow University, Suzhou, Jiangsu, P. R. China

[3] Department of Materials and Engineering, University of Washington, Seattle, Washington, USA

Correspondence
Dana Dabiri, Department of Aeronautics & Astronautics, University of Washington, Seattle, WA 98195-2120, USA.
Email: dabiri@aa.washington.edu
Guozhong Cao, Department of Materials and Engineering, University of Washington, Seattle,Washington, USA.
Email: gzcao@uw.edu

Funding information
Army Research Office, Grant/Award Number: W911NF-18-1-0143

Abstract

We utilized a seeded growth method to synthesize SiO_2@Ag NPs with tunable plasmonic resonance peak to investigate the effect of spectral overlap between the SiO_2@Ag plasmonic resonance spectrum and the PtTFPP-based oxygen sensors' absorbance spectra on luminescence enhancement and performance optimization. An organic silicate was used as the matrix. Oxygen-sensors were produced by directly casting the mixture of NPs and dyes with silicate gels onto glass slides. Oxygen-induced spectral response of the PtTFPP was obtained as the analytical signal. Our results show that when the plasmonic resonance spectrum of SiO_2@Ag has a maximum wavelength overlap with the absorbance spectra of dyes, the Stern-Volmer slopes were enhanced by almost an order of magnitude. At 21% O_2, the Stern-Volmer plot achieved a maximum seven-fold increase over the oxygen sensor without the metal-enhanced luminescence. Our results also show that 10% wt NPs is the optimal amount for the PtTFPP-SiO_2@Ag based oxygen sensors that can eliminate self-quenching and the NRET process. These data confirm that the spectral overlap between the dyes and noble metal NPs and how to eliminate self-quenching and the NRET process are vital to high-sensitive oxygen sensors. We have also shown that our fabrication process of these oxygen sensors is repeatable.

KEYWORDS
luminescence enhancement, overlap, oxygen sensors, sensitivity, tunable plasmonic resonance peak

1 | INTRODUCTION

Oxygen is closely involved with almost all living organism and is therefore one of the most important chemical species on earth. In this regard, precise measurements of its concentration are thus crucial.[1–3] Towards this end, over the past several decades, oxygen sensors have been developed in the past several decades, owing to their much-needed applications in a wide number of fields including biology, life sciences, aerospace, agricultural industry, oceanography, and environmental sciences.[4–6] In general, oxygen sensors can be divided into three types

based on different measurement mechanisms: pressure, electrochemistry and luminescence quenching.[7–10] The most common systems for oxygen sensing are based on either electrochemical devices such as the Clark electrode [7] or optical oxygen sensors.[8] The operation of Clark electrodes is based on the electrical current change in response to the O_2 reduction reaction. While one of the disadvantages for Clark electrodes is that they consume O_2 and are limited to a point analysis of samples during measurements; they are also unable to map out the O_2 distribution as well as not being suitable for small volumes for single cell study.[10] Luminescence-based oxygen sensors, on the other hand, have growth rapidly and are replacing the Clark electrode as they are easily miniaturized, disposable, non-invasive, and simple to process. Unlike electrode-based sensors, optical oxygen sensors are based on luminescence quenching, where excited-state luminophores transfer energy to surrounding O_2 molecules, thereby preventing luminescence.[1] Although considerable progress has been made recently in the optical sensing field, the development of ultra-sensitive O_2 detection techniques using luminescence oxygen sensors are still limited by their interaction with the binders they within which they are embedded.[11]

Metal enhanced fluorescence (MEF) has previously been used to increase luminescence intensity and dye sensitivity for oxygen measurements.[12–14] The utilization of MEF in oxygen sensors can therefore be an efficient method to improve the luminescence intensity and sensitivity of oxygen sensors. The higher sensitivity and enhancement of fluorescence intensity of MEF-based oxygen sensors can be mainly attributed to the augmentation of emission due to local field enhancement effects and the increased emission rate by surface plasmon coupled emission, which can increase both the quantum yield and the fluorescence intensity.[15–17] The local surface plasmon resonance (LSPR) coupled fluorescence enhancement is a complicated process and impacted by a variety of parameters, including sizes and morphologies of the metal nanoparticles (NPs) and dyes,[18–33] distance between the metal surface and the dye,[19,20] maximum spectral overlap of the metal LSPR with the excitation spectra and no overlap with emission spectra of the dye.[21] As previous reported by Ozturk,[14] when the absorbance spectra of noble metal NPs overlap with the emission spectra of dyes, the light emitted by the dyes can be re-absorbed by the noble metal NPs, a process called the inner filter effect, resulting in decreased luminescence density. Therefore, controlling and tuning the LSPR of metal NPs to achieve maximum overlap with the excitation spectra of the dye and minimum overlap with the emission spectra of the dye is a key to higher sensitivity and fluorescence intensity of MEF-based oxygen sensors.

The concept of MEF can also be extended to metal enhanced phosphorescence (MEP).[34–38] Phosphorescence is a phenomenon similar to fluorescence. The molecule can undergo intersystem crossing from the singlet excited state to the triplet excited state. The emission of a photon when the molecule relaxes from the lowest excited triplet state to the singlet ground state gives rise to phosphorescence.[37] In the presence of noble metals, nonradiative energy-transfer is thought to occur from the excited state to the surface plasmon, which in turn radiates the emission efficiently to give rise to MEP.[38] While, there are few reports about MEP in oxygen sensors. In our effort to develop an ultra-sensitive oxygen sensor, we focused on investigating the influence of the overlap between LSPR and the excitation spectra of phosphorescent dyes on the response to the variation of oxygen. For the oxygen sensor test, we use platinumtetra (pentafluorophyenyl) porphine (PtTFPP), which is a commercial phosphorescent dye that has excellent photostability and good quantum yields [12] and organically modified silicate matrix, also called the sol-gel matrix, synthesized in-house.[39] Chu et al.[12] have reported that SiO_2@Ag core-shell NPs embedded in silicate gel as an optical oxygen sensor has a higher sensitivity. Based on their results, we also choose SiO_2@Ag sample to tune the absorbance peak over a wide spectral and investigate the influence of the spectra overlap between LSPR and the excitation spectra of dyes on the performance of the oxygen sensors. In order to finely tune the plasmonic resonance, we first deposit different amounts of THPC-Au seeds and then implement the seeded growth procedure.[40,41] The subsequent growth not only decreases the interparticle separation gradually but also enhances the plasmonic coupling, leading to the formation of Ag particles with large absorption cross-section, which can maximize the absorption of incident visible and near-IR illuminations. Then we further take advantage of the tunable plasmonic resonance of the samples and demonstrate its application in oxygen sensors to optimize the sensitivity and intensity of the phosphorescent optical oxygen sensors.

2 | RESULTS AND DISCUSSION

2.1 | Structure of SiO_2@Ag

In this work, we use the seeded growth recipe to prepare SiO_2@Ag nanospheres.[42,43] To facilitate the growth of continuous and uniform Ag nanoshells on the silica surface, 300 nm SiO_2 NPs are firstly modified with polyethylenimine (PEI) [42] and then attached with THPC-Au seeds for the seeded growth of Ag nanoshells.[43] In order to precisely tuning the plasmonic peak of

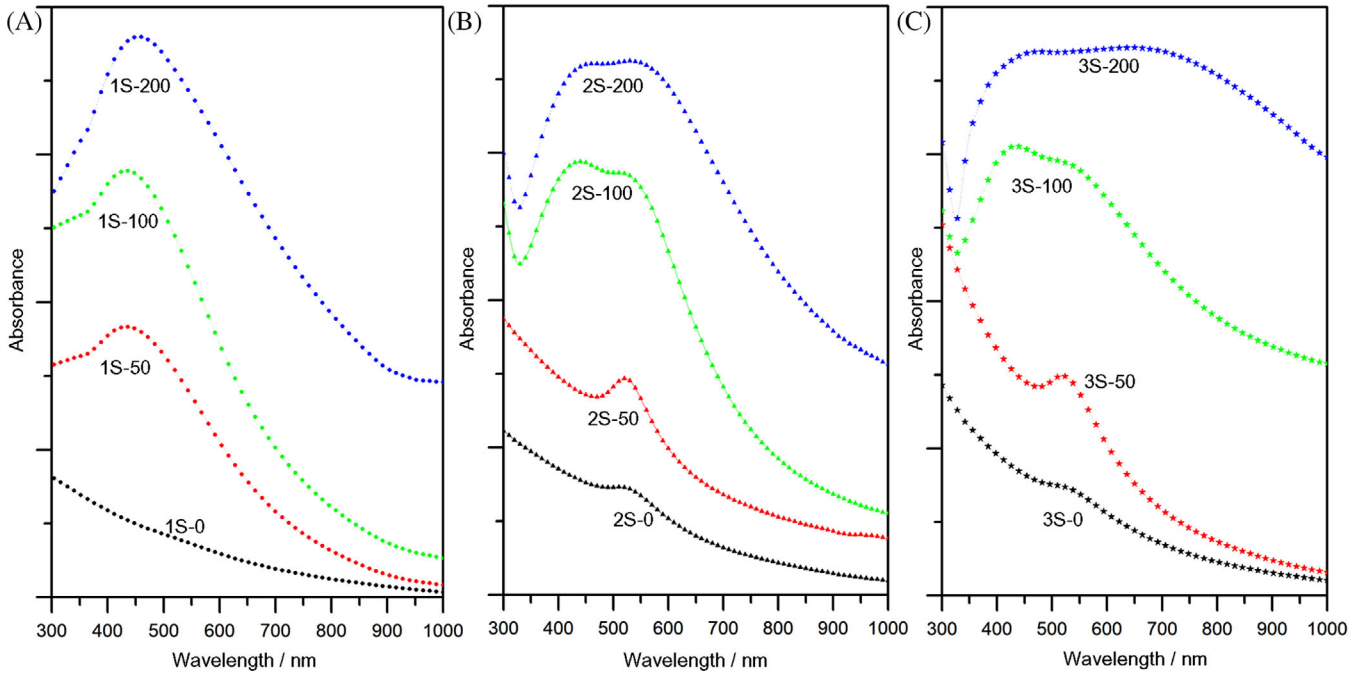

FIGURE 1 UV-Vis spectra of SiO_2@Ag synthesized through loading different amounts of THPC-Au seeds on SiO_2 nanospheres (A) 5 mL Au; (B) 30 mL Au; (C) 120 mL Au. In each figure, each line is the UV-vis spectrum of SiO_2@Ag prepared by the reaction of SiO_2@Au with 0(S-0), 50(S-50), 100(S-100), and 200(S-200) μL 0.1 M $AgNO_3$

SiO_2@Ag NPs, we mixed the PEI modified SiO_2 (0.1 g) with different amount of THPC-Au (5 mL, 30 mL, 120 mL). As shown in Figure 1A-C, there is no absorbance peak of SiO_2 attached with 5 mL THPC-Au seeds (1S-0).A small peak around 530 nm appeared and increased with an increasing amount of THPC-Au seeds (2S-0 and 3S-0), which was attributed to the coupling or aggregating of a large quantity of Au seeds.[44] Once the reduction of Ag^+ was initiated, the absorbance peak of Ag appeared and became boarder as the volume of $AgNO_3$ solution increased. The seeded growth gradually increased the Ag particles size and shortened the interparticle distance, enhancing the plasmonic coupling, finally leading to the wide absorption of incident visible wavelengths. With less THPC-Au seeds attaching to the silica surface, the absorbance peak of SiO_2@Ag (**1S-50 and 1S-100**) localized at 450 nm. As the volume of $AgNO_3$ solution increased to 200 μL (1S-200), the absorbance increased while still centered at 450 nm. The main reason for this was that there were so fewer Au seeds on the silica surface that the interparticle distance was too far to couple with each other. Therefore, the resulting absorbance peak corresponds to absorbance of separated Ag NPs on the SiO_2 surface.[45,46] With more Au seeds loaded onto the silica surface, another peak at 530 nm appeared, as illustrated by the black line (**2S-0 and 3S-0**), which corresponds to the absorbance of Au caused by the aggregating of THPC-Au seeds; adding more $AgNO_3$, the peak of Ag at 450 nm appeared and increased. Sample 2S-100 (Figure 1B) has a strong absorbance between 400 and 600 nm. Mixing with 120 mL THPC-Au seeds, the sample 3S-200 (Figure 1C) exhibited a wide absorption spectrum in the visible light, indicating that Ag shell on the surfaces of silica nanospheres created hot-spot structures on the SiO_2@Ag NPs. The diversity in the size of Ag particles and strong coupling of Ag particles on the silica surface produce the continuous spectrum of resonant multimode.[47] Through varying the loading amount of Au seeds and the volume of silver nitrate solution, we can tune the size and interparticle distance of silver NPs on the surface of SiO_2, and in this manner, we are able to control the plasmonic coupling of silver NPs. By this method, SiO_2@Ag with different absorbance peak in the visible lights can be synthesized.

In this work, the diameter of SiO_2 nanospheres prepared was about 300 nm (Figure 2A). After attaching 5 mL Au seeds on the surface and seeded growth with 100 μL $AgNO_3$, as shown in Figure 2B, there are few small Ag particles (~10 nm) on the surface, where the distance between the seeded NPs is larger than 30 nm (this distance can also be seen in Figure 2A and is also calculated using FDTD as shown in Figure 5A). For this sample, this is a large distance for the Ag plasmonic coupling to occur, which is well matched with the UV-Vis absorbance of separated Ag NPs. With the increment of the loading amount of Au seeds and volume of $AgNO_3$, as shown in Figure 2C-D, the size of the Ag particles is about 10 and 25 nm, respectively. It can be

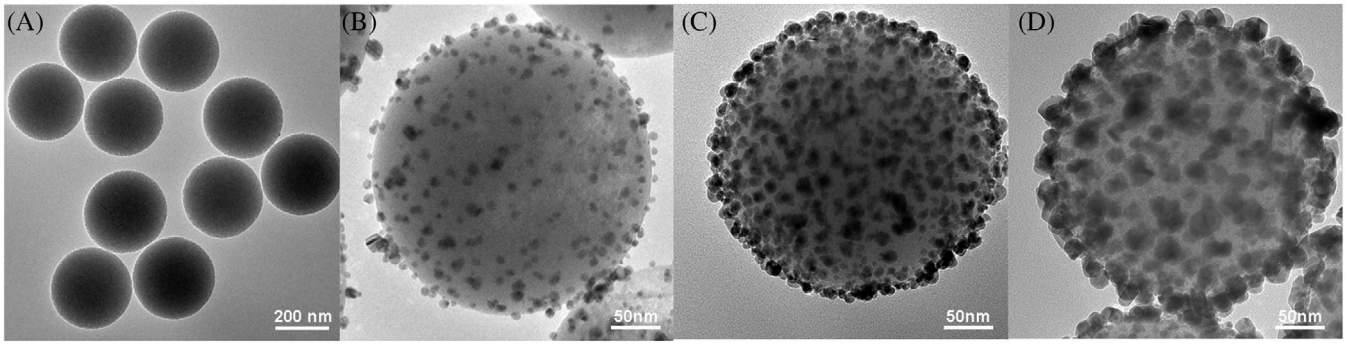

FIGURE 2 TEM images of (A) SiO_2, (B) 1S-100, (C) 2S-100, (D) 3S-200 SiO_2@Ag

clearly seen that the density and size of Ag NPs increased with an increasing amount of Au seeds and $AgNO_3$, while the nano-spacing between the Ag seed NPs on the surface of SiO_2 nanospheres decreased. As illustrated in Figure 2, from left to right, the number and size of the Ag NPs can be varied through this method. The SiO_2 can be sparsely coated with small Ag NPs (Figure 2B), or uniform and densely coated Ag NPs (Figure 2D).

2.2 | Performance of PtTFPP-SiO_2@Ag oxygen sensors

The absorption spectrum of the PtTFPP, a phosphorescent dye, has a Soret band (S_0 to S_2 transition) at 392 nm and two Q bands (S_0 to S_1 transition) at 508 and 541 nm, respectively.[41] The emission spectrum of PtTFPP has a center peak at 650 nm.[12] PtTFPP-based oxygen sensors presented in the literature have embedded the PtTFPP indicator in either a polymer[48,49] or a sol-gel matrix.[50–56] Studies have also reported that the sol-gel matrix is an ideal matrix, since it can improve the response and sensitivity of PtTFPP-based oxygen sensors due to their porous structure.[12] Therefore, in our work, we prepared the Pt-based oxygen sensors with the sol-gel matrix. For comparison, we also prepared Pt-based oxygen sensors without the sol-gel matrix. Our results for the sol-gel matrix samples are shown in Figure 3. As shown in Figure 3A, the emission intensity of Pt-based oxygen sensors with the sol-gel matrix is about three-fold higher than that of the sensors without the sol-gel matrix at 0% O_2, while, at 21% O_2, the intensities are almost same. For the oxygen sensors mixed with the SiO_2@Ag NPs (3S-100), it can be seen that the intensity of the PtTFPP-NPs oxygen sensors without the matrix is about four-fold higher than that of PtTFPP-based oxygen sensors without the matrix throughout the 0–21% O_2 range. In the sol-gel matrix, the intensity for PtTFPP-NPs oxygen sensors is four-fold higher than that of PtTFPP-oxygen sensors at 0% O_2 and almost the same at 21% O_2. It can therefore be seen that the enhancement of the emission intensity of Pt-based oxygen sensors with NPs is different with and without the sol-gel matrix.

In the simplest scenario of a luminophore in a homogeneous environment, the quenching effect can be described by the Stern-Volmer equation[21]:

$$Io/I = 1 + K_{SV}\,[O_2]\,, \tag{1}$$

where Io and I represent the steady-state luminescence intensities in the absence and presence, respectively, of the quencher (O_2 in the current case), K_{SV} is the Stern-Volmer quenching constant, and $[O_2]$ is the oxygen concentration. The slope of the Stern-Volmer plot, K_{SV}, is a measure of the sensitivity of the oxygen sensors.[12] Figure 3B shows the corresponding Stern-Volmer plots for PtTFPP-based oxygen sensors with and without SiO_2@Ag NPs and sol-gel matrix (in this work, Io is the intensity of sensors at 0% oxygen concentration). The slope of the PtTFPP-NPs oxygen sensors without the matrix is the same as that of PtTFPP-based oxygen sensors without matrix even though the slope of PtTFPP-NPs oxygen sensors in sol-gel matrix is four-fold higher than that of PtTFPP-oxygen sensors in sol-gel matrix. This demonstrates that the matrix greatly effects the intensity enhancement of the oxygen sensors. The reason may be attributed to that the diffusion of oxygen and dyes adsorbed by the NPs surface are affected in the sol-gel matrix, which can result in the different enhancement factor of oxygen sensors at different oxygen concentrations. This will be one of the topics of our future research.

Based on the theory that the intensity of luminescence is highly dependent on the spectral overlap between the metal LSPR and the excitation spectra of the dye, we compare and test the emission spectra of PtTFPP-based oxygen sensors mixed with the 1S-100, 2S-100, and 3S-200; these emission spectra are shown in Figure S1. The relative phosphorescence intensities spectrum of the PtTFPP-based oxygen sensors is also compared. For the fabrication of all the PtTFPP-based oxygen sensors with and without NPs, we use the same method. The spectra data in

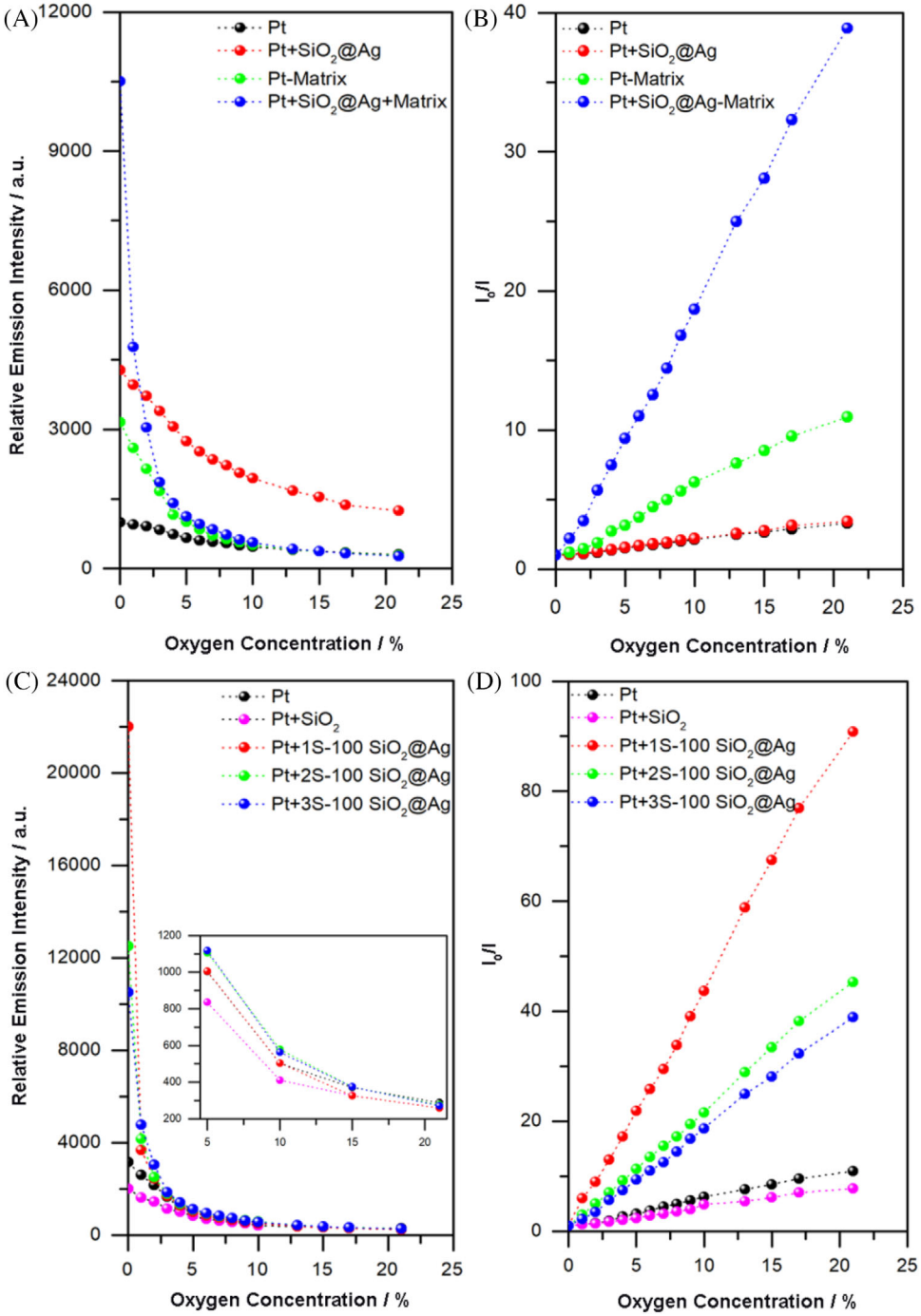

FIGURE 3 A, Emission intensity and (B) Stern-Volmer plots for PtTFPP-based oxygen sensor and PtTFPP & MEP-oxygen sensor mixed with SiO_2@Ag NPs in no matrix and sol-gel matrix for different oxygen concentrations (0-21%); (C) Emission intensity and d Stern-Volmer plots for PtTFPP-based oxygen sensors mixed with SiO_2@Ag NPs in silica sol-gel matrix for different oxygen concentration (0-21%)

Figure 3C illustrate that the relative phosphorescence intensities of oxygen sensors decrease as the oxygen concentration increases. In addition, at 21% O_2, the intensities of PtTFPP-based oxygen sensors and PtTFPP-based oxygen sensors with 1S-100 sample are almost the same; while at 0% O_2, they are 3150 and 22,000, respectively; the O_2-quenching sensitivity of the oxygen sensor with 1S-100 sample is ~7-fold higher than that of the PtTFPP-based oxygen sensors. At 21% O_2, the phosphorescence intensity profiles of the 2S-100, and 3S-200 based oxygen sensors (Figure 3D), are also almost the same as that of PtTFPP-based oxygen sensors with 1S-100; when the oxygen concentration is reduced to 0%, the phosphorescence intensities of the 2S-100, and 3S-200 based oxygen sensors

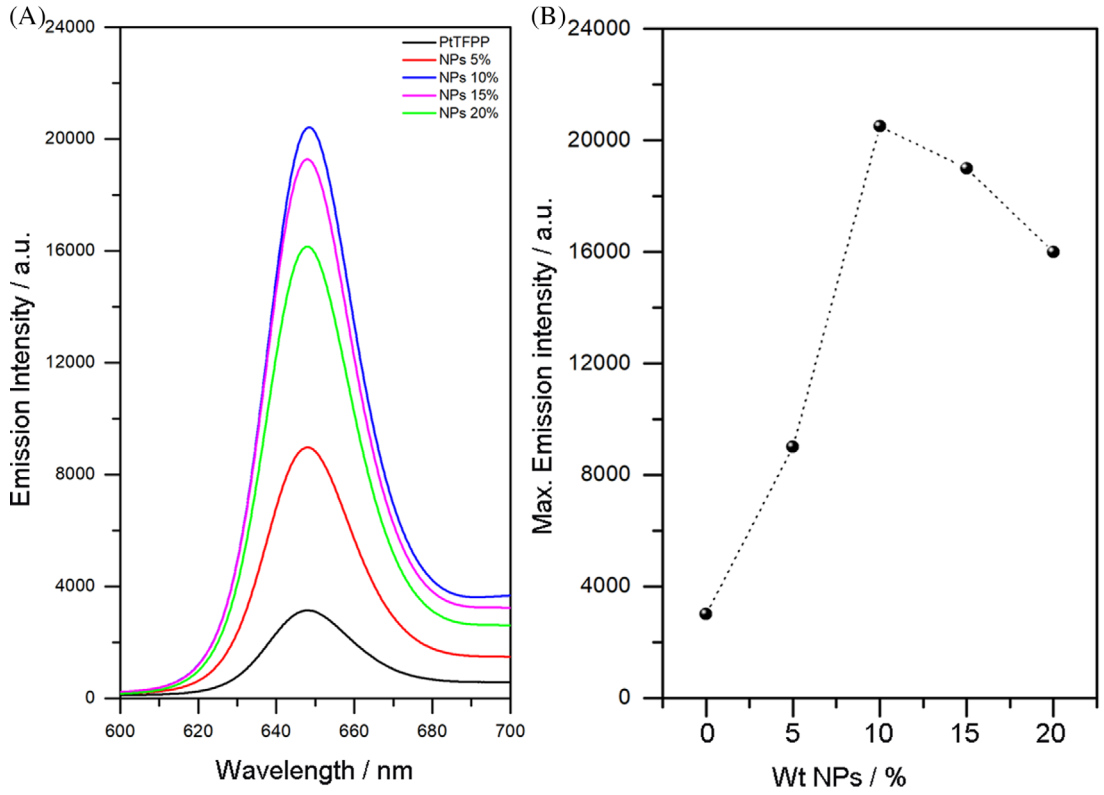

FIGURE 4 A, Emission intensity and (B) Maximum Emission intensity of PtTFPP mixed with different volume of SiO_2@Ag(S-100) at 0% oxygen concentration

are 12,500 and 10,500, respectively. The corresponding sensitivities are 3.9- and 3.3-fold higher than that of the PtTFPP-based oxygen sensors, respectively. When the concentration of O_2 is less than 5%, the phosphorescence intensities of PtTFPP-SiO_2@Ag based oxygen sensors are much higher than that of PtTFPP-based oxygen sensors, which can also be seen in the emission spectra in Figure S1. The PtTFPP-SiO_2@Ag based oxygen sensors not only have good sensitivities at a low concentration of oxygen but also exhibit bright emission, which can be utilized to measure the variation of oxygen at extreme low concentration of oxygen. The slope of the PtTFPP-based oxygen sensor is $K_{SV} = 0.56$ (0-21% oxygen concentration), which is almost the same as Chu's results.[13] The slopes of the Stern-Volmer plots for the PtTFPP-based oxygen sensors with 1S-100, 2S-100 and 3S-200 are 4.3, 2.2, and 1.8, respectively. It can also be seen that among these different SiO_2@Ag samples, the 1S-100 mixed with PtTFPP dyes in the sol-gel matrix exhibits the highest sensitivity for oxygen sensing. As a contrast, we also compared the PtTFPP-based oxygen sensors mixed with SiO_2 nanospheres. Both the intensity and slope of this sample are lower than that of PtTFPP-based oxygen sensors, which indicates that the enhancement is due to the metal-enhanced luminescence (MEL) of Ag. The different sensitivities of these samples can be mainly attributed to the absorbance peak of different SiO_2@Ag NPs, namely, the spectra overlap between the dyes and LSPR of SiO_2@Ag NPs. As mentioned above, the main absorbance of PtTFPP is localized at 392 nm. Compared with the UV-Vis spectra of these SiO_2@Ag samples, the 1S-100 sample has the maximum overlap, resulting in the highest sensitivity (Figure S2). These data provide supportive experimental evidence that the phosphorescence intensity of dyes enhanced with the SiO_2@Ag strongly relies on the overlap between the LSPR of the NP with excitation spectra properties of the dye. Considering the inner filter effect proposed by Li et al.,[15] the less overlap between the LSPR of 1S-100 and the emission spectra of PtTFPP is also a key to the highest sensitivity. Our results further confirmed that controlling and tuning the LSPR of metal NPs to make sure a maximum overlap with the excitation spectra of the dye and minimum overlap with the emission spectra of the dye is an efficient method to higher sensitivity and enhancement of luminescence intensity of MEP-based oxygen sensor.

In order to maximize the response performance of MEP-enhanced PtTFPP-based oxygen sensors, we further investigate the phosphorescence intensity of oxygen sensors with different amount of S-100 at 0% O_2concentration. As illustrated in Figure 4A, the phosphorescence intensity of PtTFPP-based oxygen sensors (fixed volume of 0.2 mg mL^{-1} PtTFPP at 0.2 mL) at 0% O_2concentration is about 3000.

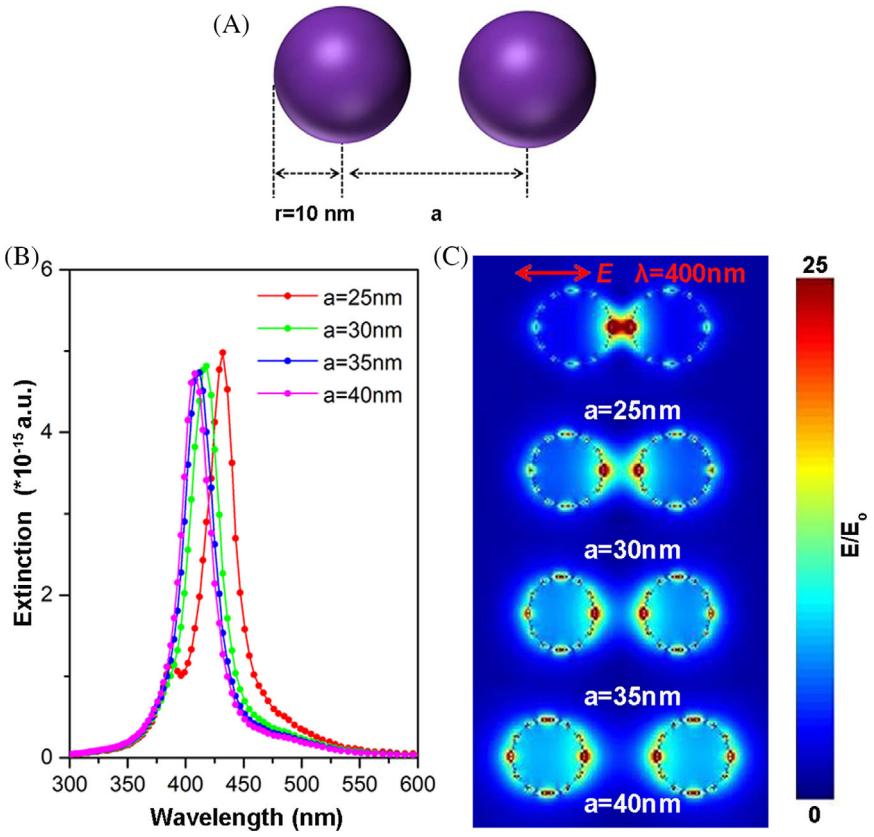

FIGURE 5 A, Schematic illustration of the model considered in FDTD simulation. B, Simulated extinction profile of two AgNPs with different gap. C, Near electromagnetic field of two AgNPs with different gap excited by 400 nm incident light

After mixing S-100 NPs in the PtTFPP-based oxygen sensors, the phosphorescence intensity is greatly enhanced. With an addition of 5% and 10% wt S-100 solution, the intensities are as high as 9000 and 21,000, respectively. When the amount of S-100 solution further increased to 15% and 20% wt, the phosphorescence intensity decreased to 19,000 and 16,000, respectively. The trend can be clearly seen in the maximum phosphorescence intensity of Figure 4B. The data show that the intensity of PtTFPP-MEL based oxygen sensors is highly related to the amount of SiO_2@Ag NPs. One possible explanation for this effect can be ascribed to the self-quenching of phosphorescence and non-radiative energy transfer (NRET) to the NPs. Self-quenching of luminescence is due to the resonance energy transfer between dyes (homo RET). In the case of fluorescein, the Forster distances for homo RET is about 42 Å[59]; RET is expected to occur when a macromolecule contains more than a single dye. When the molecular distance is too close, the luminescence emitted will self-quench and lead to a weaker emission intensity. In MEL systems, when the dye is closer to the noble metal NPs, there will be non-radiative energy transfer from the excited state of dyes to the NPs, which will lead to luminescence quenching. When this distance is sufficiently large, the energy transfer can be eliminated, and at the same time, the emission under the effect of the electromagnetic field of NPs will be greatly enhanced (see discussion in Section 2.3). In this case, when the number of NPs is 5% wt, the amount of NPs is not enough to enhance the luminescence of all of the dye. The luminescence of segments of the dye that are not enhanced can lead to more self-quenching and less MEL. As the number of NPs increases to 10% wt, most of the dye is impacted by the MEL of the NPs, leading to greater luminescence. When the number of NPs is further increased to 15% and 20% wt, the NRET is dominated by the NPs, resulting in the decrease of intensity. In this case, 10% wt NPs is the optimal amount for the PtTFPP-SiO_2@Ag based oxygen sensors. Therefore, optimizing the inter-NP distance by varying the number of NPs eliminates self-quenching and the NRET process, thereby making this vital to developing highly luminescence and ultra-sensitive oxygen sensors.

2.3 | Finite-difference time-domain method (FDTD)

To further investigate the plasmonic coupling's influence in MEL-based oxygen sensors, we use two AgNPs as a simplified model to simulate the coupling via different interparticle distances through finite-difference time-domain method.[40] As schematically shown in Figure 5A, the diameter of AgNPs and interparticle distance are set at 20 and 25–40 nm, respectively. Figure 5B shows the

extinction spectra of two AgNPs via interparticle distance. When the interparticle distance is set at 40 nm, the extinction spectra of AgNPs exhibits a sharp peak at about 400 nm; the extinction spectra red-shifts once the interparticle distance shorten; when the interparticle distance is 25 nm, the extinction peak of AgNPs red-shifts to around 430 nm. These data indicate that as the interparticle gap decreases, the plasmonic coupling becomes strong and the plasmonic peak red-shifts. The interparticle plasmonic coupling can also be visualized in the FDTD solution by using a two-dimensional frequency-domain field profile. As shown in Figure 5C, when the incident light with wavelength of 400 nm irradiates the AgNPs along the X-axis, the near electromagnetic field shows great enhancement at the 25 nm gap; while at the 40 nm, there is no coupling. These data show that the plasmonic coupling can enhance the electromagnetic field, while shifting the peak away from 400 nm. Given that the laser beam excitation is at 400 nm, plasmonic coupling leads to the extinction peak shift far from the excitation laser's wavelength and also the maximum absorption peak of PtTFPP dyes, thereby resulting in less enhancement of luminescence. Therefore, the sample with a maximum absorption around 400 nm will exhibit the largest luminescence enhancement, which is consistence with our experiment data: our results with the S-100 sample with smaller AgNPs (~10 nm) and larger interparticle distance (≥30 nm) exhibits the best performance in MEP-enhanced oxygen sensors. The simulation data also suggest that fine tuning the interparticle distance of silver NPs on silica nanospheres can maximize the loading amount of Ag NPs to increase the enhancement factor and at the same time prevent the excessive density of Ag NPs' distribution on the surface of SiO_2 that will lead to the interparticle coupling, which is unfavorable in this system. In order to confirm the repeatability for the preparation of oxygen sensors, we use the same recipe for the preparation of PtTFPP-1S-100 SiO_2@Ag oxygen sensors and then test their emission intensity through the 0–21% O_2 range. The intensities of 1–5# oxygen sensors in Figure S3 are almost the same as that shown in Figure 3A. The data further show that our method to fabricate oxygen sensors with high sensitivity is repeatable.

3 | CONCLUSION

We have demonstrated that the sensitivity of PtTFPP-NPs-based oxygen sensor is highly dependent on the spectral overlap between the absorption spectra of the dyes and plasmonic resonance spectrum of the noble metal NPs. When these spectra have maximum overlap, the Stern-Volmer O_2-quenching sensitivity at 0% O_2 (I_o/I) is seven-fold higher than that of the PtTFPP-based oxygen sensor sensitivity, which is the highest reported in this study. In addition, we optimized the number of NPs to eliminate self-quenching and the NRET process. The MEP-enhanced PtTFPP-based oxygen sensor using SiO_2@Ag NPs demonstrates very high sensitivities through the O_2 range studied. This increased sensitivity, which is almost an order of magnitude, will result in more accurate measurements, thereby demonstrating that combining MEP with the PtTFPP-based oxygen sensor is a viable approach to enhancing the performance of oxygen sensors and that MEP-oxygen sensors hold a promising future in the field of oxygen sensors. In conclusion, we have also demonstrated that the spectral overlap between the dyes and noble metal NPs and how to eliminate self-quenching and the non-radiative energy transfer (NRET) process affects the sensitivity of these oxygen sensors, thereby providing us with a guide for the design of MEP-oxygen sensors for different applications.

4 | EXPERIMENTAL SECTION

4.1 | Synthesis of SiO_2 nanospheres

Colloidal silica nanospheres were prepared through a modified Stober method.[42] In a typical synthesis for ~300 nm particles, 4.5 mL TEOS was mixed with 45.5 mL ethanol, and then added into a mixture solution containing 28 mL ethanol, 15 mL water, and 7 mL aqueous solution of ammonia (28% wt). After stirring for 2 hours at room temperature, the silica particles were collected by centrifugation, washed with ethanol and water, and then re-dispersed in 20 mL water. As the TEM image shows in Figure 2A, the silica NPs are spherical with a diameter about 300 nm.

4.2 | Synthesis of SiO_2@Ag

Disperse 0.6 g SiO_2 in 60 mL PEI (1% wt.) solution and stir for 4 hours.[43] Then the SiO_2 nanospheres were washed with water for three times and dissolved in 6 mL water (0.1 g mL^{-1}). After that, 1 mL sample was pipetted to 5–120 mL THPC-Au seed solution under sonication for 1 hour and stirring overnight. Then, the solution was centrifuged and dispersed in water. The THPC-Au seed was synthesized using Baiker's method: A mixture of 1.35 mL NaOH (0.2 M), 41 mL water, 0.90 mL tetrakis-(hydroxymethyl) phosphonium chloride (THPC) aqueous solution (1.2 mM) was prepared and stirred for 10 minutes, to which 1.80 mL aqueous solution of chloroauric acid (25 mM) was added quickly.[42] The final solution was aged at 4°C for at least 2 weeks before use.

For synthesis of SiO_2@Ag, a solution of 10 mL H_2O, 10 mL Trisodium citrate (0.1 M), 10 mL acetonitrile, 2 mL ascorbic acid (0.1 M), and 1 mL SiO_2@Au seed (30 mg mL^{-1}) was sonicated for 5 minutes, then 0.25-2.00 mL $AgNO_3$(0.1 M) was added under sonication for 10 minutes. Finally, the sample was centrifuged and washed with water for three times.

4.3 | Fabrication of MEL-enhanced oxygen sensor using SiO_2@Ag with sol-gel matrix

We chose the Octyl-triEOS/TEOS composite sol-gel as the matrix material and prepared by mixing Octyl-triEOS (0.20 mL) and TEOS (4.00 mL) to form a precursor solution according to Chu's method.[12] EtOH (1.25 mL) and HCl (0.1 M, 0.40 mL) were then added to the sol-gel solution to catalyze the ORMOSIL reaction. The resulting solution was stirred magnetically for 1 hour at room temperature. Then 0.10 mL Triton-X-100 was added to improve the homogeneity of the silica sol. 20 mg SiO_2@Ag was added to 0.20 mL PtTFPP/EtOH (0.2 mg mL^{-1}) solution and stirred for 12 hours. Then 0.50 mL composite sol-gel solution was added to the dye solution. Finally, the solution was capped and stirred magnetically for another 12 hours. Before the test, 200 μL sol-gel solution was dropped onto glass slide (2 × 2 cm^2) and left to stabilize under ambient conditions for 24 hours.

ACKNOWLEDGMENTS

The authors gratefully acknowledge the financial support provided by the U.S. Army Research Office under Grant No. W911NF-18-1-0143 overseen by Dr. Matthew Munson.

CONFLICT OF INTERESTS

The authors declare no conflict of interest.

DATA AVAILABILITY STATEMENT

Research data are not shared.

ORCID

Dana Dabiri https://orcid.org/0000-0003-3573-6897

REFERENCES

1. X. D. Wang, O. S. Wolfbeis, *Chem. Soc. Rev.* **2014**, *43*, 3666.
2. G. L. Semenza, *Science* **2007**, *318*, 62.
3. Y. Y. Mao, Y. Gao, S. S. Wu, S. Wu, J. Shi, B. Zhou, Y. Tian, *Sensors Actuators B* **2017**, *251*, 495.
4. R. C. Evans, P. Douglas, *ACS Appl. Mater. Interfaces.* **2009**, *1*, 1023.
5. A. Mills, *Chem. Soc. Rev.* **2005**, *34*, 1003.
6. M. I. J. Stich, S. Nagl, O. S. Wolfbeis, U. Henne, M. A. Schaeferling, *Adv. Funct. Mater.* **2008**, *18*, 1399.
7. R. Xue, C. Ge, K. Richardson, A. Palmer, M. Viapiano,, J. J. Lannutti, *ACS Appl. Mater. Interfaces.* **2015**, *7*, 8606.
8. B. Lei, B. Li, H. Zhang, S. Lu, Z. Zheng, W. Li, Y. Wang, *Adv. Funct. Mater.* **2006**, *16*, 1883.
9. D. B. Cybyk1, B. M. Reinsch, K. F. Presley, R. M. Schweller, A. Tedeschi, T. Burns, F. J. Chaparro, J. T. Ly, M. J. Dalton, M. Lozano, T. A. Grusenmeyer, J. J. Lannutti, *Med Devices Sens.* **2021**,*4*,10149.
10. C. J. Lim, S. Lee, J. H. Kim, H. J. Kil, Y. C. Kim, J. W. Park, *ACS Appl. Mater. Interfaces.* **2018**, *10*, 41026.
11. R. Liu, T. Xiao, W. Cui, J. Shinar, R. Shinar, *Anal. Chim. Acta.* **2013**, *778*, 70.
12. C. S. Chu, T. W. Sung, Y. L. Lo, *Sensors Actuators B* **2013**, *185*, 287.
13. K. Aslan, J. R. Lakowicz, H. Szmachiski, C. D. Geddes, *J. Fluorescence* **2015**, *15*, 37.
14. O. Ozturk, O. Oter, S. Yildirim, E. Subasi, K. Ertekin, E. Celik, H. Temel, *J. Luminescence*. **2014**, *155*, 191.
15. J. F. Li, C. Y. Li, R. F. Aroca, *Chem. Soc. Rev.* **2017**, *46*, 3962.
16. T. Ribeiro, C. Baleizao, J. S. Farinha, *Sci. Rep.* **2017**, *7*, 2440.
17. Z. Qu, P. Duan, J. Zhou, Y. Wang, M. Liu, *Nanoscale* **2018**, *10*, 985.
18. T. Ming, L. Zhao, Z. Yang, H. J. Chen, L. D. Sun, J. F. Wang, C. H. Yan, *Nano Lett.* **2009**, *9*, 3896.
19. P. Reineck, D. Gomez, S. H. Ng, M. Karg, T. Bell, P. Mulvaney, U. Bach, *ACS Nano* **2013**, *7*, 6636.
20. K. Aslan, M. Wu, J. R. Lakowicz, C. D. Geddes, *J. Am. Chem. Soc.* **2007**, *129*, 1524.
21. H. Yuan, S. Khatua, P. Zijlstra, M. Yorulmaz, M. Orrit, *Angew. Chem., Int. Ed*. **2013**, *52*, 1217.
22. S. Yin, T. Yao, T. Wu, Y. Zhang, P. Wang, *Talanta* **2017**, *174*, 14.
23. Y. Mao, Z. Liu, L. Liang, Y. Zhou, Y. Qiao, Z. Mei, B. Zhou, Y. Tian, *ACS Omega* **2018**, *3*, 5669.
24. L. Feng, M. Liu, H. Liu, C. Fan, Y. Cai, L. Chen, M. Zhao, S. Chu, H. Wang, *ACS Appl. Mater. Interfaces.* **2018**, *10*, 23647.
25. M. A. Badshah, J. Ju, X. Lu, N. Abbas, S. Kim, *Sensors Actuators: B. Chemical.* **2018**, *274*, 451.
26. J. Liu, S. Li, V. R. Bhethanabotla, *ACS Sens.* **2018**, *3*, 222.
27. E. Kohr, B. I. Karawdeniya, J. R. Dwyer, A. Gupta, W. B. Euler, *Phys. Chem. Chem. Phys.* **2017**, *19*, 27074.
28. I. G. Theodorou, Q. Jiang, L. Malms, X. Xie, R. C. Coombes, E. O. Aboagye, A. E. Porter, M. P. Ryan, F. Xie, *Nanoscale* **2018**, *10*, 15854.
29. A. Camposeo, L. Persano, R. Manco, Y. Wang, P. D. Carro, C. Zhang, Z. Li, D. Pisignano, Y. Xia, *ACS Nano* **2015**, *9*, 10047.
30. H. Yuan, Y. Lu, Z. Wang, Z. Ren, Y. Wang, S. Zhang, X. Zhang, J. Chen, *Chem. Commun.* **2016**, *52*, 1808.
31. C. A. Orozco, J. G. Liu, M. W. Knight, Y. Wang, J. K. Day, P. Nordlander, N. J. Halas, *Nano Lett.* **2014**, *14*, 2926.
32. K. Sugawa, T. Tamura, H. Tahara, D. Yamaguchi, T. Akiyama, J. Otsuki, Y. Kusaka, N. Fukuda, H. Ushijima, *ACS Nano* **2013**, *7*, 9997.
33. T. Zhou, L. Lin, M. Rong, Y. Jiang, X. Chen, *Anal. Chem.* **2013**, *85*, 9839.
34. J. C. Ostrowski, A. Mikhailovsky, D. A. Bussian, M. A. Summers, S. K. Buratto, G. C. Bazan, *Adv. Funct. Mater* **2006**, *16*, 1221.
35. S. Pan, L. J. Rothberg, *J. Am. Chem. Soc.* **2005**, *127*, 6087.

36. R. Rajeev, E. Esimbekova, M. Kirillova, V. Kratasyuk, *Anal. Chim. Acta* **2017**, *971*, 1.
37. Y. Zhang, K. Aslan, M. Previte, S. N. Malyn, C. D. Geddes, *J. Phys. Chem. B.* **2006**, *110*, 25108.
38. N. J. Halas, S. Lal, W. S. Chang, S. Link, P. Nordlander, *Chem. Rev.* **2011**, *111*, 3913.
39. C. S. Chu, Y. L. Lo, T. W. Sung, *Talanta* **2010**, *82*, 1044.
40. Y. Xia, K. D. Gilroy, H. C. Peng, X. Xia, *Angew. Chem., Int. Ed.* **2017**, *56*, 60.
41. C. Zhu, J. Zeng, J. Tao, M. C. Johnson, I. Schmidt-Krey, L. Blubaugh, Y. Zhu, Z. Gu, Y. Xia, *J. Am. Chem. Soc.* **2012**, *134*, 15822.
42. W. Stober, A. Fink, E. Bohn, *J. Colloid Interface Sci.* **1968**, *26*, 62.
43. J. Chen, J. Feng, Z. Li, P. Xu, X. Wang, W. Yin, M. Wang, X. Ge, Y. Yin, *Nano Lett.* **2019**, *19*, 400.
44. D. G. Duff, A. Baiker, P. P. Edwards, *Langmuir* **1993**, *9*, 2301.
45. C. Gao, J. Vuong, Q. Zhang, Y. Liu, Y. Yin, *Nanoscale* **2012**, *4*, 2875.
46. C. Gao, Q. Zhang, Z. Lu, Y. Yin, *J. Am. Chem. Soc.* **2011**, *133*, 19706.
47. X. Liu, Y. Yin, C. GAO, *Langmuir* **2013**, *29*, 10559.
48. Y. Amao, T. Miyashita, I. Okura, *J. Fluorine Chem.* **2001**, *107*, 101.
49. S. K. Lee, I. Okura, *Anal. Commun.* **1997**, *34*,185.
50. I. Klimant, F. Ruckruh, G. Libsch, C. Stangelmayer, O.S. Wolfbeis, *Mikrochim. Acta* **1999**, *131*, 35.
51. A. N. Watkins, B. R. Wenner, J. D. Jordan, W. Y. Xu, J. N. Demas, F. V. Bright, *Appl. Spectrosc.* **1998**, *52*, 750.
52. Y. Tang, E. C. Tehan, Z. Tao, F. V. Bright, *Anal. Chem.* **2003**, *75*, 2407.
53. R. M. Bukowski, R. Ciriminna, M. Pagliaro, F. V. Bright, *Analytical Chemistry* **2005**, *77*, 2670.
54. X. H. Yang, L. R. Peng, L. B. Yuan, P. P. Teng, F. J. Tian, L. Li, S. Z. Luo, *Opt. Commun.* **2011**, *284*, 3462.
55. T. S. Yeh, C. S. Chu, Y. L. Lo, *Sensors Actuators B: Chemical* **2006**, *119*, 701.
56. C. S. Chu, Y. L. Lo, *Sensors Actuators B: Chemical* **2007**, *124*, 376.
57. B. J. Basu, *Sensors Actuators B: Chemical* **2007**, *123*, 568.
58. C. S. Chu, Y. L. Lo, *Sensors Actuators B: Chemical* **2011**, *155*, 53.
59. J. R. Lakowicz, J. Malicka, S. D. Auria, I. Gryczynski, *Anal. Biochem.* **2013**, *320*, 13.

AUTHOR BIOGRAPHIES

Dr. Wenwen Yin is the postdoc research of aeronautics & astronautics at the University of Washington. She received her Ph.D. from Fudan University (China) and was a visiting Ph.D. student at University of California, Riverside for 2 years. Dr. Yin's research is the development of functional nanostructured materials for photonic, catalytic, and energy applications through unique tools including chemical synthesis, surface functionalization, and self-assembly techniques. At present, she is developing high sensitive optical oxygen sensors with novel methods.

Dr. Dabiri is the Professor of Aeronautics and Astronautics at the University of Washington. He obtained his doctorate degree at the University of California at San Diego. Dr. Dabiri's interest is to advance the study of fundamental fluid flows through new and advanced quantitative flow imaging techniques. He has contributed to the highly successful DPIV (Digital Particle Image Velocimetry) technique and played a pivotal role in the team that pioneered the three-component version of the DPIV technique (DDPIV). He has also contributed to the 3D-DPTV (Digital Particle Tracking Velocimetry) technique. At present, he is continuing development in novel methods in 2D and 3D particle tracking velocimetry, and simultaneous global pressure, temperature, and velocimetry measurements, for applications in studies of aerodynamics, hydrodynamics, laminar and turbulent boundary layers, transition, separation, flow control, experimental approaches to turbulence modeling, wake flows, and micro-flows, cardiovascular flows and aero-acoustics.

Dr. Guozhong Cao is the Boeing-Steiner Professor of Materials Science and Engineering and Adjunct Professor of Chemical and Mechanical Engineering at the University of Washington. He received his Ph.D. from Eindhoven University of Technology (the Netherlands). Dr. Cao has published over 200 refereed papers, and authored and edited four books and three conference proceedings on nanotechnology. Dr. Cao serves as editor of *Annual Review of Nano Research* and associate editor of *Journal of Nanophotonics*. His current research is focused mainly on nanomaterials for energy related applications, such as solar cells, lithium-ion batteries, supercapacitors, and hydrogen storage. Other research includes scintillation oxides, nanobiosensors, PZT-based microelectromechanical (MEMS) devices.

SUPPORTING INFORMATION

Additional supporting information may be found online in the Supporting Information section at the end of the article.

How to cite this article: W. Yin, J. Chen, J. Sui, D. Dabiri, G. Cao. *Nano Select* **2021**, *2,* 2451. https://doi.org/10.1002/nano.202100131